

# Molecular Dynamics on Interface and Nanoscratch Mechanisms of Alkanethiol Self-Assembled Monolayers

Wen-Yang Chang,<sup>†</sup> Te-Hua Fang,<sup>\*,‡</sup> and Chun-Nan Fang<sup>‡</sup>

*Microsystems Technology Center, Industrial Technology Research Institute, Tainan 709, and Institute of Mechanical and Electromechanical Engineering, National Formosa University, Yunlin 632, Taiwan*

Received: June 8, 2009; Revised Manuscript Received: September 25, 2009

The interface dynamics and nanoscratched mechanisms of alkanethiol self-assembled monolayers (SAM) chemisorbed on a gold surface are investigated using molecular dynamics simulation. The characteristic mechanisms mainly include the nanoscratched depths, the workpiece temperatures, the scratched speed, the SAM chain lengths, and the shapes of the indenters. The simulation results show that the disorder and the plastic mobility of SAM structures increased with increasing nanoscratched depth. The scratched forces, the potential energy, the friction force, and the friction coefficient increased with increasing scratched depth. The larger scratched depth required a larger force to overcome the resistance, which leads to the increases in the friction force. The variations of the scratched forces and the friction forces after scratching at various temperatures are very similar. An increase in the scratched force, friction force, and friction coefficient with increasing scratched speed is observed. The scratched shape after scratching is clearer for a longer SAM chain. The SAM structures are easily tilted and bent when the chain length is longer. The reaction forces after scratching using a spherical indenter are higher than those after scratching using a Vickers indenter.

## 1. Introduction

Self-assembled monolayers (SAMs) have recently become a field of great interest for applications in biology,<sup>1,2</sup> physics,<sup>3</sup> optical,<sup>4,5</sup> and chemistry<sup>6</sup> sensors due to their high selectivity, stability, and sensibility.<sup>7</sup> SAMs are organized into a head group and a tail group with a functional group. The head group has special affinity for a substrate, and the tail with a functional group at the terminal end provides the functionality of the SAMs. In general, the head group of the SAM film can be formed by the spontaneous adsorption of a molecule from solution onto a metal substrate. For example, alkanethiol chains are widely used on gold surfaces<sup>8–10</sup> because gold is stable, it has a strong interaction with thiol, and it can be handled in ambient conditions. In general, the substrates tend to readily adsorb adventitious organic materials because these adsorbates lower the free energy of the interface between the metal and the ambient environment. Love et al.<sup>11</sup> presented some ideal substrates to combine with different head groups.

Studies on model construction and interface characteristics of SAMs chemisorbed on a structure surface are important for investigating the reinforcement mechanism. However, in these studies there is great difficulty in understanding the mechanical properties of the MD behaviors at the atomic scale during the experimental process. A series of atomic friction forces and adhesive forces with various end groups, chain numbers, and scanning velocities have been developed using atomic force microscopy (AFM).<sup>12,13</sup> AFM measurement is sensitive enough to obtain the interfacial functionality mechanisms of SAMs, but noise and turbulence are easily induced on the nanometer scale. Experiment tests reveal the *in situ* mechanical and processing responses of nanomaterials, but it is difficult to measure the

dynamic characteristics of SAMs at present. Atomic simulation with nanoindentation and nanoscratching<sup>14–16</sup> avoids these experimental problems and allows us to investigate the molecular trajectories, thermodynamic behaviors, and atomic mechanical characteristics, etc.

There are some contributions reported in the SAM characterization using MD simulations. For example, Cossaro<sup>17</sup> et al. studied the SAM's structure of long-chain alkyl sulfides on gold surface for MD trajectories and relative interface energy. Jia et al.<sup>18</sup> investigated the interface structures and interaction energies between alkanethiol and epoxy. Aydogmus et al.<sup>19</sup> conducted a molecular simulation of self-assembled monolayers with alkyl functionality on the surfaces of a mesoporous inorganic substrate. Few studies have focused on the molecular dynamic characteristics of sliding friction and transfer reactions using MD simulation.<sup>20,21</sup>

In this study we investigate the force effect of SAMs chemisorbed on a gold surface at various nanoscratched depths, workpiece temperatures, chain lengths of the SAMs, and shapes of the indenters. The scratched force, friction forces, friction coefficients, potential energy, and deformation mechanism of the SAM film were studied for analyzing interface dynamics and nanoscratched mechanisms of SAMs chemisorbed on a gold surface during the nanoscratched process. The aim of this study is to provide further insight into the dynamic characteristics of the SAM chains using the nanoscratched mechanism.

## 2. Simulation Model and Methodology

**2.1. SAM Model and Boundary Condition.** Figure 1 shows the SAM model for MD scratching simulation consists of two fixed layers, a thermostat, an Au surface, and a SAM film. The dimensions of the model sizes in the *x*, *y*, and *z* directions are 11.22, 12.04, and 3.06 nm, respectively, using a face-centered-cubic (fcc) bulk lattice. Periodic boundary conditions were enforced in the *x* and *y* directions. There was no periodic boundary condition along the *z* direction. The two atomic layers

\* To whom correspondence should be addressed. E-mail: fang.tehua@msa.hinet.net. Phone: +886-5-631 5395.

<sup>†</sup> Industrial Technology Research Institute.

<sup>‡</sup> National Formosa University.

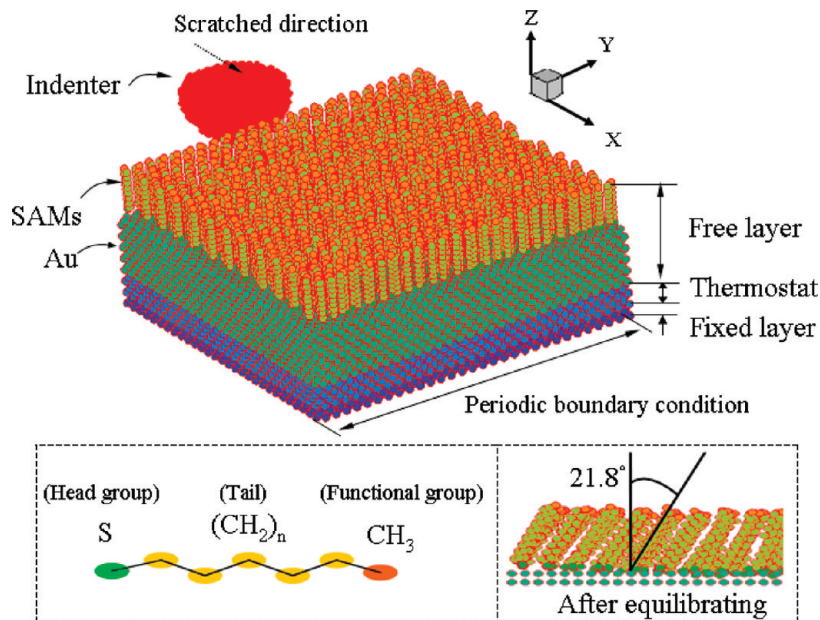


**Figure 1.** Model of SAMs chemisorbed on a nanoscale gold film for nanoscratching simulation.

at the bottom were fixed in space to prevent the substrate from being moved; the degrees of freedom were constrained in displacement, bond interactions, and rotation of the atoms. Four layers of thermostat atoms were set above the fixed layers to depict surface atoms influenced by sulfur atoms during thermovibration. The Au surface was the (100) plane with an fcc lattice and 26880 atoms. The SAMs,  $(S(CH_2)_nCH_3)$ , with various numbers of  $CH_2$  groups were simulated to investigate the characteristics of the alkanethiol molecules. SAMs with an array of  $24 \times 24$  were chemisorbed on the Au surface, with S,  $CH_2$ , and  $CH_3$  as the head group, the tail, and the functional group, respectively, as shown in Figure 1. Initially, the molecules were all-trans and arranged with a spacing of 0.5 nm to the nearest-neighbor distance of the triangular lattice formed by the sulfur head groups on the Au surface. For structural models, we assumed that the gold surface remains flat and free of dislocation defects during the MD simulation. The  $CH_2$  and  $CH_3$  groups were treated as a single-spherical molecule for simplicity, giving 17 united molecules per chain. The spherical indenter was a hemispherical probe that consisted of 1136 diamond atoms. The Vickers indenter consisted of 2992 diamond atoms in the form of a square-based pyramid with an angle of  $22^\circ$  between the indenter face and the contact surface. Both indenters were assumed to be a rigid object during the simulation process. The spherical and Vickers indenters were initially placed on the outside of the SAM model and then moved to the scratched depth. The indenter was moved and scratched the SAM surface along the  $x$  direction at a fixed height. The boundary condition of temperature for all atoms was initially 300 K. The SAM model was equilibrated to its minimum energy configuration at 300 K before the scratching of the MD simulation. Constant nanoscratching depth and scratching velocity were maintained.

**2.2. Potential Energy.** For interactions of the potential energy models, standard force fields were used to evaluate all-atom force fields for the conformational energy of the alkanethiol chain. The total conformational energy of the force fields includes bond stretching, bond bending, torsion, nonbonding, and surface interaction. The bond interactions of stretching, bending, and torsion between SAM chains were calculated using a general universal force field,  $E_{\text{bond}}$ , to characterize the interactions by the classical potential.<sup>22</sup> The binding potential

energy of the sulfur head group on the Au substrate was estimated using the Morse potential,  $E_{\text{Morse}}$ . The second-moment approximation for the tight-binding (TB-SMA) many-body potential,<sup>23</sup>  $E_{\text{TB-SMA}}$ , has been proven capable of reproducing a variety of experimental observations<sup>24,25</sup> for the interaction of Au atoms. The Lennard-Jones potential function,  $U_{\text{LJ}}$ , was employed to describe interaction among the indenter, the SAMs, and the Au atoms.

The total interactomic potential of the conformational energy for interface dynamics is given by

$$E_{\text{total}} = E_{\text{Morse}} + U_{\text{LJ}} + E_{\text{bond}} + E_{\text{TB-SMA}} \quad (1)$$

The Morse potential energy,  $E_{\text{Morse}}(r_{ij})$ , can be described as

$$E_{\text{Morse}}(r_{ij}) = D(e^{-2\alpha(r_{ij}-r_0)} - 2e^{-\alpha(r_{ij}-r_0)}) \quad (2)$$

where  $D$ ,  $r_0$ , and  $r_{ij}$  are the cohesion energy of the exchange interaction, the equilibrium distance, and the separation distance between atoms  $i$  and  $j$ , respectively.  $\alpha$  is fitted to the bulk modulus of the material. The values of the potential parameters for SAM atoms are listed in Table 1.<sup>26–30</sup>

The Lennard-Jones potential model with terms of a short-range 6–12 for the calculation process is<sup>24</sup>

$$U_{\text{LJ}}(r_{ij}) = 4\epsilon \left[ \left( \frac{\sigma}{r_{ij}} \right)^{12} - \left( \frac{\sigma}{r_{ij}} \right)^6 \right] \quad (3)$$

where  $U_{\text{LJ}}(r_{ij})$  is a pair potential function and  $\epsilon$  and  $\sigma$  represent the well depth of the potential and the distance at which the interatomic potential is zero, respectively.  $r_{ij}$  is a distance between atoms  $i$  and  $j$ . The potential parameters of the Lennard-Jones potential for SAM atoms are shown in Table 1.

The bonded interactions of the alkanethiol chain include the bond stretching,  $E_s(r_{ij})$ , the bond angle bending,  $E_\theta(\theta_{ij})$ , and the torsional rotational,  $E_d(\varphi_{ijkl})$ , potentials. The potential energy of the bond stretching interactions between sites  $i$  and  $j$  was assumed to be harmonic. The bond angle bending represents

**TABLE 1: Potential Parameters of the Force Field for SAM Simulation**

$E_{\text{Morse}}(r_{ij})$					
chain	$r_0$ (nm)	$\alpha$ (nm $^{-1}$ )	$D_e$ (kJ/mol)		
Au–S	0.256	0.1477	13.3		
$U_{\text{LJ}}(r_{ij})$					
chain	$\sigma$ (nm)		$\epsilon$ (kJ/mol)		
Au	0.2935		0.039		
S	0.425		1.6629		
CH <sub>2</sub>	0.3905		0.495		
CH <sub>3</sub>	0.3905		0.7325		
$E_s(r_{ij})$					
chain	$r_0$ (nm)	$k_s$ [kJ/(mol nm $^2$ )]			
CH <sub>2</sub> –S	0.182	132600			
CH <sub>2</sub> –CH <sub>2</sub>	0.153	132600			
CH <sub>3</sub> –CH <sub>3</sub>	0.153	132600			
$E_\theta(\theta_{ijk})$					
chain	$\theta_0$ (deg)	$k_\theta$ [kcal/(mol rad $^2$ )]			
Au–S–CH <sub>2</sub>	100.0	63.0			
CH <sub>2</sub> –CH <sub>2</sub> –S	114.4	62.5			
CH <sub>2</sub> –CH <sub>2</sub> –CH <sub>2</sub>	109.5	63.0			
CH <sub>2</sub> –CH <sub>2</sub> –CH <sub>3</sub>	109.5	63.0			
$E_d(\varphi_{ijkl})$					
chain	$a_1$ (kJ/mol)	$a_2$ (kJ/mol)	$a_3$ (kJ/mol)	$a_4$ (kJ/mol)	$a_5$ (kJ/mol)
all	9.28	12.16	−13.12	−3.06	−31.50
$E_{\text{TB-SMA}}(r_{ij})$					
chain	$p$	$q$	$\xi$ (eV)	$A$ (eV)	$r_0$ (nm)
Au–Au	10.23	4.036	1.790	0.206	2.884

the interaction among three consecutively bonded sites  $i, j$ , and  $k$ , and was also assumed to be harmonic energy. The torsional rotational potential between four sites,  $i, j, k$ , and  $l$ , is the change in the equilibrium dihedral angles. The total bonded interaction is given by

$$E_{\text{bond}} = E_s(r_{ij}) + E_\theta(\theta_{ijk}) + E_d(\varphi_{ijkl}) \\ = \frac{1}{2}k_s(r_{ij} - r_0)^2 + \frac{1}{2}k_\theta(\theta_{ijk} - \theta_0)^2 + \sum_{i=1}^5 a_i \cos^i(\varphi_{ijkl}) \quad (4)$$

where  $k_s$  and  $k_\theta$  are the force constants and  $r_0$  and  $\theta_0$  are the equilibrium distance and the equilibrium bond angle, respectively.  $a_i$  and  $\varphi_{ijkl}$  are the potential parameter and the dihedral angle, respectively. The potential parameters of  $E_{\text{bond}}$  for the SAM atoms are shown in Table 1.

The TB-SMA potential energy,  $E_{\text{TB-SMA}}(r_{ij})$ , has the following repulsive pair potential and cohesive bond energy term:

$$E_{\text{TB-SMA}}(r_{ij}) = \sum_{i=1}^N \left[ - \sum_j \xi^2 \exp \left[ - \left( 2q \left( \frac{r_{ij}}{r_0} \right) \right)^{1/2} \right] + A \exp \left[ - p \left( \frac{r_{ij}}{r_0} - 1 \right) \right] \right] \quad (5)$$

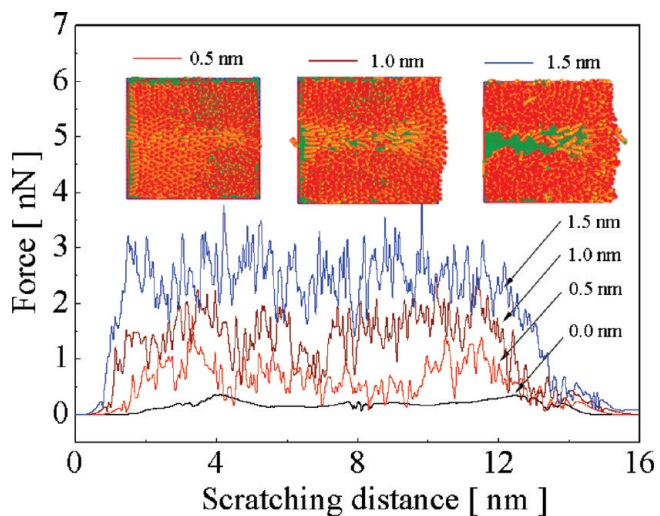


**Figure 2.** Nanoscratched forces of the SAM film at scratched depths of 0.0, 0.5, 1.0, and 1.5 nm.

where  $\xi$ ,  $r_0$ , and  $N$  are the effective hopping integral, the first-neighbor distance, and the number of atoms considered, respectively. The terms  $\xi$ ,  $q$ ,  $p$ , and  $A$  are fitted to the experimental values of the cohesive energy. The parameters of the  $E_{\text{TB-SMA}}$  potential function for Au–Au interactions are listed in Table 1.

### 3. Results and Discussion

Atomistic deformation mechanisms of SAMs chemisorbed on nanoscale gold films after nanoscratching were observed, including the effects of the scratched depths, the workpiece temperatures, the scratched speeds, the SAM chain lengths, and the indenter's shapes. These characteristic mechanisms were mainly simulated using the MD method to clarify SAM deformation, scratched loads, friction forces, friction coefficients, and the potential energy for various values of the parameters. The characteristic mechanisms for atomic interfaces and potential energy after scratching are given as follows.

**3.1. Effect of Nanoscratched Depths.** For the MD scratched simulation, the chain length and the number of SAM layers were 17 and 1, respectively. The scratched depths during MD simulation include 0, 0.5, 1.0, and 1.5 nm at a scratched velocity of 100 m/s and at a constant temperature of 300 K. The scratched depth of 0 nm means that the indenter was defined as the point at which the force between the SAM surface and the indenter becomes repulsive as the tip approaches the surface for investigating the effect of the friction on the SAM critical surface. Before the MD scratched simulation, the SAM model was equilibrated to obtain an ordered arrangement. The tilt angle of the SAM chains after equilibration was about 21.8° from the surface normal, as shown in Figure 1.

Figure 2 shows the scratched force curves that summarize three orientations for a SAM chemisorbed on a gold surface at the scratched depths of 0, 0.5, 1.0, and 1.5 nm. After scratching, a steady state is reached such that the forces are essentially constant, fluctuating around an average value. There is a ploughing effect during the scratched motion of the indenter. In the inset of Figure 2, the SAM surface after scratching was almost not damaged when the scratched depth was less 0.5 nm. However, the SAM chains easily piled up in front of the indenter at the scratched depth of 1.5 nm. The disorder and the plastic mobility of the SAM structures increased with increasing scratched depth. The SAM structures have higher vibration of

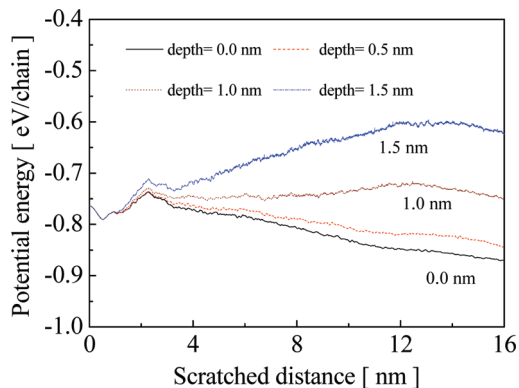


**Figure 3.** Potential energy versus scratched distance at scratched depths of 0.0, 0.5, 1.0, and 1.5 nm.

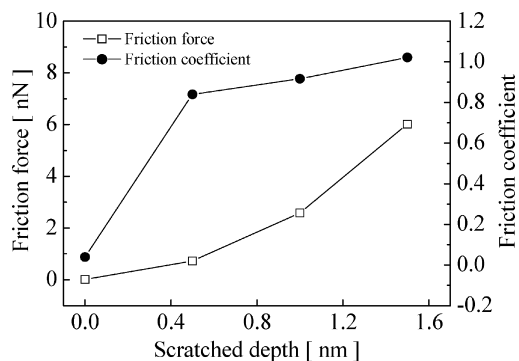


**Figure 4.** Friction force and friction coefficient between the SAM film and the indenter after scratching at the different depths.

plastic deformation after scratching. The scratched shape formed according to the indenter geometry, with SAMs displaced to the periphery of the contact. Therefore, the scratched forces increased with increasing scratched depth. SAM chains begin to change orientation and to deform with increasing scratched depth due to the scratching. The SAM structure deformation changes from elastic to plastic when the scratched depths are increased. The elastic deformation means that SAM chains can self-recover to their original conformation after scratching.

The indenter surface has a potential energy that makes the SAM straighten and stretch when the indenter begins to scratch the SAM surface.<sup>31</sup> The potential energy was then converted to repulsive energy due to the van der Waals force. The repulsive energy increased with increasing contact area between the SAMs and the indenter. The repulsive energy is the interatomic potential which prevents the collapse of molecules. The potential energy was calculated by summing the compression, bending, torsion, and van der Waals energies for Morse, TB-SMA, and Lennard-Jones potential energies. Figure 3 shows the potential energies of the scratched motion on the SAM surface at the scratched depths of 0, 0.5, 1.0, and 1.5 nm. Results showed that the potential energy increased with increasing scratched depth. This is due to the fact that a larger scratched depth has a larger structural recovery. The bond interactions between the SAM chains, the binding potential energy of the sulfur head group on the Au substrate, the interaction of Au atoms, and the interaction among the indenter, the SAMs, and the Au substrate atoms all increased with increasing scratching depth.

Figure 4 shows the friction force and the friction coefficient for a SAM film at various scratched depths. The friction force is resisting the relative lateral motion of the SAM chains at the equilibrated configuration after indenter scratching. The friction coefficient between the SAM chains and the indenter is defined

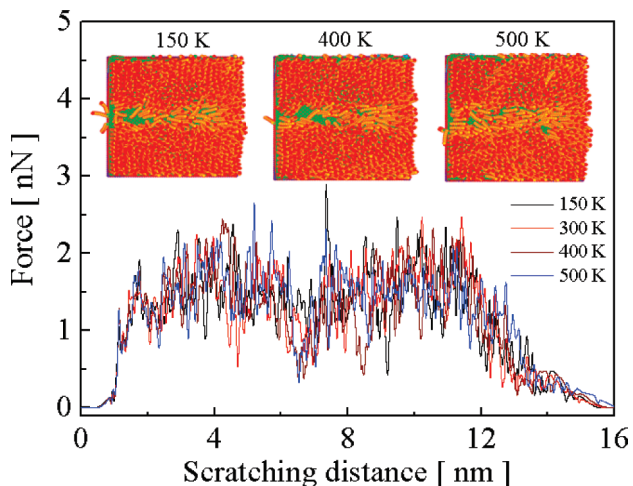


**Figure 5.** Scratched forces of the SAM film after scratching depths of 1.0 nm at temperatures of 150, 300, 400, and 500 K.

as the ratio of the tangential force divided by the normal force. The friction forces at the scratched depths of 0, 0.5, 1.0, and 1.5 nm were 0.009, 0.725, 2.585, and 6.017 nN, respectively. The friction coefficients at the scratched depths of 0, 0.5, 1.0, and 1.5 nm were 0.039, 0.840, 0.917, and 1.021, respectively. The friction force and the friction coefficient increased with increasing scratched depth. Therefore, the bond stretching, angle bending, and torsional rotational potentials of the alkanethiol chains decreased as the scratching depth increased. This is due to the fact that a larger scratched depth required a larger force to overcome the resistance, which leads to the increases in the friction force.

**3.2. Effect of Workpiece Temperatures.** The lateral mobility of the head groups of the SAMs on the gold substrate at the various workpiece temperatures was observed. The mobility involves the absorbed strength and stretching force of the SAM films. To better characterize the structural and functional characteristics of a SAM, the scratched force, potential energy, friction force, and friction coefficient of SAMs chemisorbed on the gold surface after scratching at the temperatures of 150, 300, 400, and 500 K were investigated. During MD simulation, the chain length and the number of SAM layers were 17 and 1, respectively. The SAM model was also equilibrated to its minimum energy configuration before the scratching simulation. The scratched depth and the scratching velocity were 1.0 nm and 100 m/s, respectively. Constant nanoscratching depth and scratching velocity were maintained during the entire scratching length.

Figure 5 shows the scratched force curves of dynamic motion along the scratching distance at the temperatures of 150, 300, 400, and 500 K. The scratched forces at the beginning and at the end of scratching were almost zero. For all cases, the fluctuating variations of the scratched forces after scratching at various temperatures were very similar. Although the bond forces of the SAM chains at higher temperature were weak, the scratched force was seemingly temperature independent. This can be attributed to the fact that the plastic deformation is governed by the mechanical yield strength. However, SAM chains were distorted and removed along the scratched direction, even scratching at the lower temperature situation; see the inset of Figure 5. As a result, an abrasive groove was formed on the SAM film, and an accumulation of pile-up along the lateral side of the indenter was also found. The shape after scratching at the scratched end is not apparent due to a smaller accumulation effect. The curves of the potential energy of the SAMs after

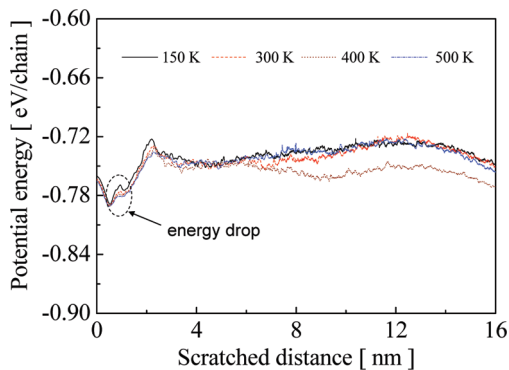


**Figure 6.** Potential energies of the SAM film after scratching at temperatures of 150, 300, 400, and 500 K.

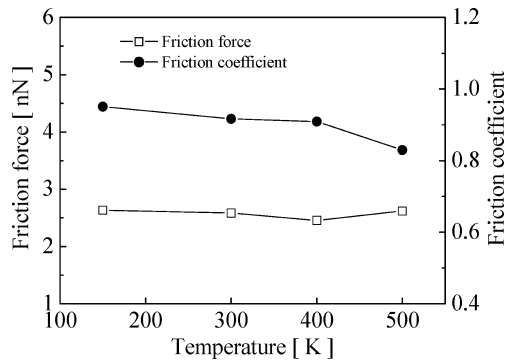
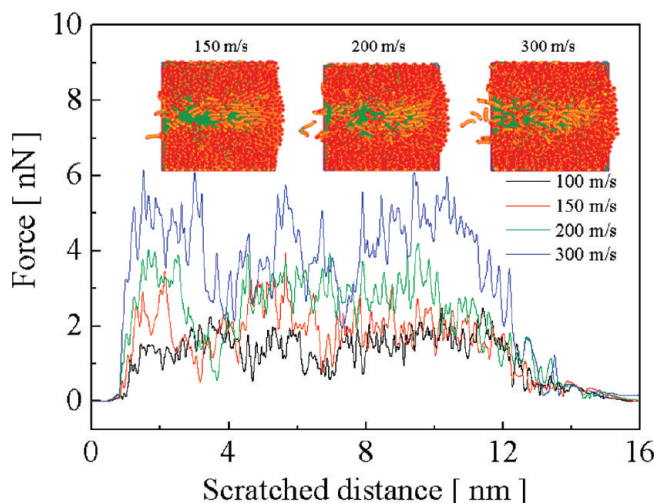


**Figure 7.** Friction forces and friction coefficients after scratching at various temperatures.

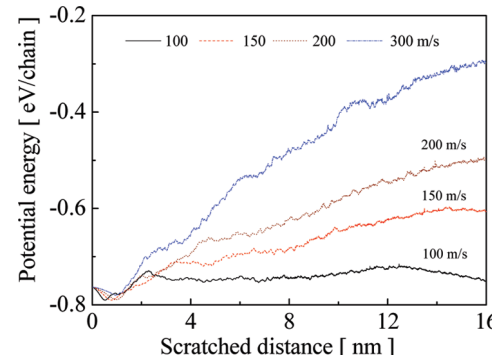
scratching at various temperatures had an energy drop at the scratched distance of about 1.1 nm due to chain slipping relaxation, as shown in Figure 6. The effect of the potential energy after scratching at various workpiece temperatures was not apparent. It can be expected that the average tilt angle of the SAM chains initially increased with increasing workpiece temperature after equilibrating to its minimum energy configuration.<sup>32</sup>

Figure 7 shows the friction force and the friction coefficient of the SAMs after scratching at the temperatures of 150, 300, 400, and 500 K. The friction forces at the temperatures of 150, 300, 400, and 500 K are 2.635, 2.585, 2.456, and 2.620 nN, respectively. The friction force was observably temperature independent. It was expected that the SAM chains were similar to the pillars and had a smaller difference of the friction force during scratching due to the increasing average tilt angle after SAM equilibration. This result is in good agreement with the characteristics of the scratched force simulation above. The friction coefficients at the temperatures of 150, 300, 400, and 500 K are 0.951, 0.917, 0.910, and 0.830, respectively. The friction coefficients slightly decreased with increasing temperature. As can be expected, both normal and tangential forces were somewhat different, although the change was smaller for different temperatures.

**3.3. Effect of the Scratched Speed.** In general, the scratched speed for MD simulation is higher than for the experimental testing.<sup>33</sup> This is one of the drawbacks of MD simulation, producing spurious effects. To study the effects of the scratched speed on the SAM surface, the scratch speeds include 100, 150, 200, and 300 m/s for investigating mechanical characteristics and interchain interactions among the SAM layers, the gold atoms, and the substrate. During MD simulation, the scratched depth, the chain length, the temperature, and the number of SAM layers were 1.0 nm, 17, 300 K, and 1, respectively. Before



**Figure 8.** Force versus scratched distance for scratching speeds of 100, 150, 200, and 300 m/s after a scratching depth of 1.0 nm at a temperature of 300 K.



**Figure 9.** Potential energy of the SAM film at scratching speeds of 100, 150, 200, and 300 m/s.

scratching, the SAM models also needed to be equilibrated to get an ordered arrangement.

Figure 8 shows the scratched forces of the SAM film after scratching at various speeds. An increase in the scratched force with increasing scratched speed is observed.<sup>34</sup> The scratched speed dependence may be explained by the fact that the resistance force of the indenter in the scratched region increased as the scratching speed increased. The amplitude of the force fluctuation for higher speed scratching was relatively larger than for lower speed scratching during scratching. The disorder region and the broadening of damage after scratching at the high-speed scratching were larger than at the low-speed scratching. The broadening of damage was due to the deformation of the SAM chain along the scratched region induced by the indenter. In addition, the number of SAM chains peeled from the scratching surface was somewhat high for the higher speed scratching. There was a larger accumulation of SAM chains in front of the scratched direction for higher speed scratching. The average fluctuation force after scratching increased with increasing scratching velocity.

Figure 9 shows the potential energies of the SAM film at the scratched speeds of 100, 150, 200, and 300 m/s. A decrease in the potential energy with decreasing scratched speed was observed. The potential energies were similar for all cases at the initial scratched distance of about 2 nm before. The bond interactions between SAM chains, the binding potential energy of the sulfur head group on the Au substrate, the interaction of Au atoms, and the interaction among the indenter, the SAMs,

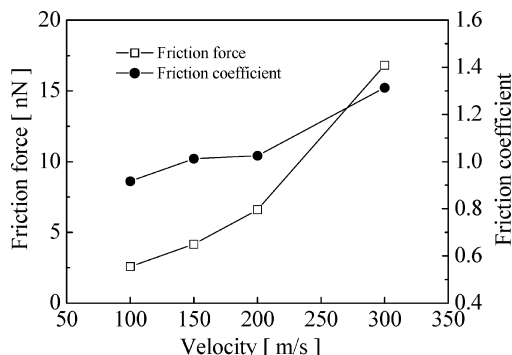


**Figure 10.** Friction forces and friction coefficients after SAM scratching at different speeds.

and the Au substrate atoms all increased with increasing scratching velocity.

The friction forces and friction coefficients between the indenter and SAM surface after scratching speeds of 100, 150, 200, and 300 m/s are shown in Figure 10. The friction forces at the scratched speeds of 100, 150, 200, and 300 m/s were 2.858, 4.153, 6.603, and 16.815 nN, respectively. The friction coefficient at scratched speeds of 100, 150, 200, and 300 m/s were 0.917, 1.012, 1.025, and 1.314, respectively. The friction force and the friction coefficient observably increased with increasing scratched speed. The friction characteristics observably depend on the scratched speed, which leads to the increase in the friction resistance. It can also be expected that the SAM chains have a larger structural recovery force at the higher speed scratching.

**3.4. Effect of the SAM Chain Length.** Another important characteristic is the SAM chain length chemisorbed on nanoscale

gold films after scratching. The interface and nanoscratched mechanisms of 1-heptanethiol ( $S(CH_2)_6CH_3$ ), dodecanethiol ( $S(CH_2)_{11}CH_3$ ), pentadecanethiol ( $S(CH_2)_{14}CH_3$ ), and 1-hexadecanethiol ( $S(CH_2)_{15}CH_3$ ) were investigated. The atomistic model was scratched using a hemispherical indenter at a velocity of 100 m/s. The number of SAM layers and the workpiece temperature were 1 and 300 K, respectively. SAM models with chain lengths of 8, 13, 16, and 17 on the gold surface were investigated. The atomistic models of the SAM were also equilibrated to get an ordered arrangement before scratching. For the effect of the SAM chain length, the mechanical characteristics and the intermolecular interactions among the SAM layers, the gold atoms, and the substrate were worth clarifying using MD simulation.

Figure 11 shows the side view and the top view of SAM deformations for SAM models with chain lengths of 8, 13, 16, and 17 after scratching. A higher degree of plastic deformation took place along the scratched region after scratching. The SAMs were malleable and releasable due to mechanical characteristics within their structures. Therefore, an abrasive groove of the SAM chains, disordered debris, and a side move were found along the lateral side of the scratched direction in all cases.

The scratched shape after scratching is clearer for longer chains. The SAM structures were easily tilted and bent when the length of the chain was longer.<sup>32</sup> The SAM chains become more disorderly and the elastic recovery is smaller for the longer chain after scratching. The broadening of damage along the scratching direction and the chain accumulation in front of the scratching for longer chains are larger than for shorter chains.

The simulation results of the scratched force, potential energy, friction force, and friction coefficient for SAM models with

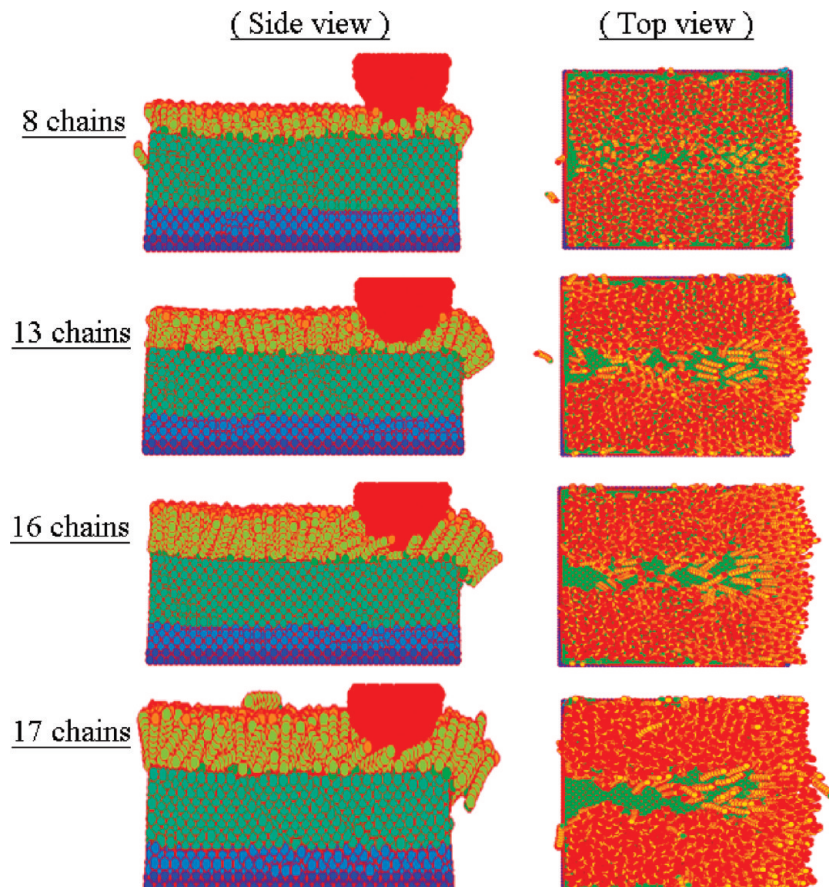


**Figure 11.** SAM deformation mechanism of the side and the top views for SAMs with chain lengths of 8, 13, 16, and 17 after scratching.

**TABLE 2: Comparison of Mechanical Characteristics for SAM Models with Chain Lengths of 8, 13, 16, and 17 after Nanoscratching**

chain length	8	13	16	17
scratched force (nN)	1.50	1.78	1.85	1.92
potential energy (eV/chain)	-0.323	-0.549	-0.630	-0.666
friction force (nN)	2.411	4.704	6.044	6.117
friction coefficient	0.367	0.675	0.838	1.021

chain lengths of 8, 13, 16, and 17 after scratching are shown in Table 2. The scratched force, friction force, and friction coefficient increased with increasing chain length. This can be attributed to the contact area between the SAM chain and the indenter increasing with increasing chain length. The contact area indirectly induced the adhesive forces during plastic deformation.<sup>35</sup> Therefore, the chain length governed the recovery force and the structural relaxation. A decrease in the potential energy with increasing SAM chain length is observed.<sup>17</sup> The potential energy contribution consists of van der Waals and surface energy terms. The van der Waals force increased with an increase of the molecular chain length. For the shorter term, the surface energy term dominates the potential energy due to entropic contribution. The shorter SAM chain observably had a substrate effect after a force was scratched on the SAM surface. The vibration of the SAM chains is large when the chain length is long.

**3.5. Effect of the Indenter Shape.** The shape of the indenter affects the scratched force and the contact area during experimental nanoscratched tests. Therefore, it is better to study the effect of the indenter's shape using MD simulation. This study simulated the characteristics of the spherical and the Vickers indenters to investigate the mechanical behavior and the underlying mechanism of surface plasticity. The Vickers indenter was a square-based pyramid. When the results of the two indenters are compared, the obtained levels of the sphere indenter for the scratched force and the potential energy are higher than those of the Vickers indenter, as shown in Figure 12. It was expected that the scratched force at which the substrate started to deform plastically is sensitive to the sphere indenter. This was due to the contact area between the indenter and the sample being large. Therefore, the scratched force increased when the shape of the indenter was smoother. The Vickers indenter is not perfect for MD simulation because of its larger deviation comparison with the spherical indenter. A correction factor related to the lack of any revolution paraboloid during MD simulation must be taken into account.<sup>36</sup> After the correction factor was applied for the Vickers indenter, the characteristic analyses of molecular deformation during MD simulation were similar to those of the Berkovich, Vickers, and conical indenters.<sup>36</sup>

After scratching, the friction forces for the spherical and Vickers indenters were 6.017 and 3.623 nN, respectively. The friction coefficients for the spherical and Vickers indenters were 1.021 and 0.893, respectively. Simulated results showed that the friction force and the friction coefficient for the spherical indenter were observably higher than for the Vickers indenter. During the scratching, the friction resistance observably depended on the contact area. Consequently, interaction forces and adhesive forces were enhanced due to the chain diffusion and pushing.

#### 4. Conclusion

A molecular dynamics simulation of alkanethiol self-assembled monolayers after nanoscratching was performed to

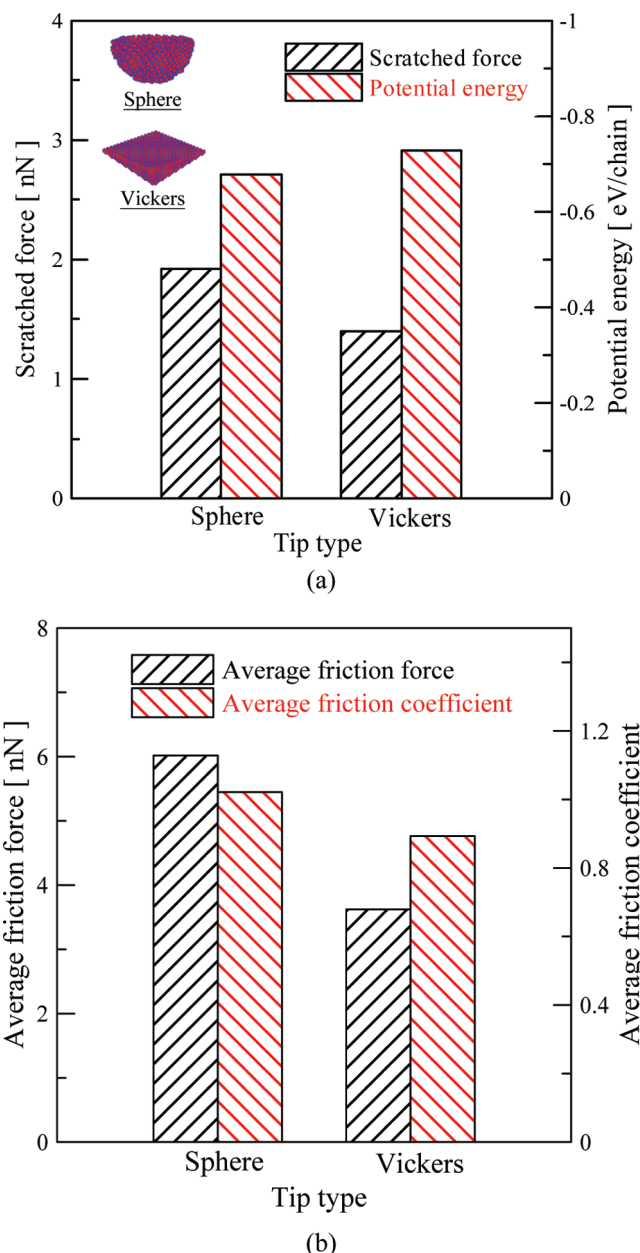


**Figure 12.** Spherical and Vickers indenters after scratching on SAM films: (a) scratched force and potential energy, (b) friction force and coefficient.

investigate the effects of the scratched depth and speed, the workpiece temperatures, the length of the SAM chain, and the shape of the indenter. The following conclusions were obtained.

- (1) The SAM chains were easily disordered and elongated after indenter nanoscratching. The scratched force and the friction force increased with increasing contact area.
- (2) A larger scratched depth and speed required a larger force to overcome the resistance due to increasing friction motion.
- (3) The potential energy increased with increasing scratched depth and speed. The discrepancy of potential energy gradually increased with increasing scratched distance.
- (4) The broadening of damage along the scratching direction and the chain accumulation in front of the scratching for longer chains were larger than for shorter chains.
- (5) The scratched speed dependence may be explained by the fact that the resistance force in the scratched region increased when the scratching speed was increased.

(6) The friction force and the friction coefficient for the spherical indenter were observably higher than for the Vickers indenter.

**Acknowledgment.** This work was partially supported by the National Science Council of Taiwan under Grant NSC 97-2221-E-150-069-MY3.

## References and Notes

- (1) Mrksich, M. *Acta Biomater.* **2009**, *5*, 832.
- (2) Matsunaga, S.; Yokomori, R.; Ino, D.; Yamada, T.; Kawai, M.; Kobayashi, T. *Electrochem. Commun.* **2007**, *9*, 645.
- (3) Henry, C. W.; Millner, P. A.; Prodromidis, M. I. *Sens. Actuators, B* **2006**, *114*, 1064.
- (4) Long, F.; He, M.; Zhu, A. N.; Shi, H. C. *Biosens. Bioelectron.* **2009**, *24*, 2346.
- (5) Li, J. C. *Chem. Phys. Lett.* **2009**, *473*, 189.
- (6) Bowen, J.; Manickam, M.; Evans, S. D.; Critchley, K.; Kendall, K. N.; Preece, J. A. *Thin Solid Films* **2008**, *516*, 2987.
- (7) Moccelini, S. K.; Fernandes, S. C.; Camargo, T. P.; Neves, A.; Vieira, I. C. *Talanta* **2009**, *78*, 1063.
- (8) Azzam, W.; Bashir, A.; Terfort, A.; Strunkus, T.; Wöll, C. *Langmuir* **2006**, *22*, 3647.
- (9) Noh, J.; Kato, H. S.; Kawai, M.; Hara, M. *J. Phys. Chem. B* **2006**, *110*, 2793.
- (10) Birss, V.; Dang, K.; Wong, J. E.; Wong, R. P. *J. Electroanal. Chem.* **2003**, *67*, 550–551.
- (11) Love, J. C.; Estroff, L. A.; Kriebel, J. K.; Nuzzo, R. G.; Whitesides, G. M. *Chem. Rev.* **2005**, *105*, 1103.
- (12) Bhushan, B.; Liu, H. *Phys. Rev. B* **2001**, *63*, 245412.
- (13) Cruz, A. L. M.; Tremont, R.; Martinez, R.; Romanach, R.; Cabrera, C. R. *Appl. Surf. Sci.* **2005**, *241*, 371.
- (14) Akabane, T.; Sasajima, Y.; Onuki, J. *J. Appl. Phys.* **2007**, *46*, 3024.
- (15) Jin, J.; Shevlin, S. A.; Guo, Z. X. *Acta Mater.* **2008**, *56*, 4358.
- (16) Komanduri, R.; Chandrasekaran, N.; Raff, L. M. *Wear* **2000**, *240*, 113.
- (17) Cossaro, A.; Mazzarello, R.; Rousseau, R.; Casalis, L.; Verdini, A.; Kohlmeyer, A.; Floreano, L.; Scandolo, S.; Morgante, A.; Klein, M. L.; Scoles, G. *Science* **2008**, *321*, 943.
- (18) Jia, J.; Huang, Y. D.; Long, J.; He, J. M.; Zhang, H. X. *Appl. Surf. Sci.* **2009**, *255*, 6451.
- (19) Aydogmus, T.; Ford, D. M. *J. Membr. Sci.* **2008**, *314*, 173.
- (20) Wu, C. D.; Lin, J. F.; Fang, T. H. *Comput. Mater. Sci.* **2007**, *39*, 808.
- (21) Fang, T. H.; Weng, C. I.; Chang, J. G. *Surf. Sci.* **2002**, *501*, 138.
- (22) Rappe, A. K.; Casewit, C. J.; Colwell, K. S.; Goddard, W. A.; Skiff, W. M. *J. Am. Chem. Soc.* **1992**, *114*, 10024.
- (23) Fang, T. H.; Chang, W. J.; Wu, C. D. *Microelectron. Eng.* **2008**, *85*, 223.
- (24) Gomez, L.; Diep, H. T. *Phys. Rev. Lett.* **1995**, *74*, 1807.
- (25) Miguel, J. J.; Miranda, R. *J. Phys.: Condens. Matter* **2002**, *14*, R1063.
- (26) Sung, I. H.; Kim, D. E. *Appl. Phys. A: Mater. Sci. Process.* **2005**, *81*, 109.
- (27) Lee, S. H.; Kim, H. S.; Pak, H. *Bull. Korean Chem. Soc.* **1998**, *19*, 1047.
- (28) Ghorai, P. K.; Glotzer, S. C. *J. Phys. Chem. C* **2007**, *111*, 15857.
- (29) Henz, B. J.; Hawa, T.; Zachariah, M. R. *Langmuir* **2008**, *24*, 773.
- (30) Tupper, K. J.; Brenner, D. W. *Langmuir* **1994**, *10*, 2335.
- (31) Fang, T. H.; Chang, W. Y.; Huang, J. J. *Acta Mater.* **2009**, *57*, 3341.
- (32) Vemparala, S.; Karki, B. B. *J. Chem. Phys.* **2004**, *121*, 4323.
- (33) Komanduri, R.; Chandrasekaran, N.; Raff, L. M. *Wear* **2000**, *240*, 113.
- (34) Bouhacina, T.; Aime, J. P.; Gauthier, S.; Michel, D. *Phys. Rev. B* **1997**, *56*, 7694.
- (35) Hu, Y. Z.; Zhang, T.; Maa, T. B.; Wang, H. *Comput. Mater. Sci.* **2006**, *38*, 98.
- (36) Sakharova, N. A.; Fernandes, J. V.; Antunes, J. M.; Oliveira, M. C. *Int. J. Solids Struct.* **2009**, *46*, 1095.

JP905389W